

Potential formation of three pyrimidine bases in interstellar regions

Liton Majumdar

Univ. Bordeaux, LAB, UMR 5804, F-33270, Floirac, France

CNRS, LAB, UMR 5804, F-33270, Floirac, France &

Indian Centre for Space Physics, Chalantika 43, Garia Station Road, Kolkata- 700084, India

Prasanta Gorai

Indian Centre for Space Physics, Chalantika 43, Garia Station Road, Kolkata- 700084, India

Ankan Das

Indian Centre for Space Physics, Chalantika 43, Garia Station Road, Kolkata- 700084, India

Sandip K. Chakrabarti

S. N. Bose National Centre for Basic Sciences, Salt Lake, Kolkata- 700098, India

&

Indian Centre for Space Physics, Chalantika 43, Garia Station Road, Kolkata- 700084, India

Received _____; accepted _____

ABSTRACT

Work on the chemical evolution of pre-biotic molecules remains incomplete since the major obstacle is the lack of adequate knowledge of rate coefficients of various reactions which take place in interstellar conditions. In this work, we study the possibility of forming three pyrimidine bases, namely, cytosine, uracil and thymine in interstellar regions. Our study reveals that the synthesis of uracil from cytosine and water is quite impossible under interstellar circumstances. For the synthesis of thymine, reaction between uracil and :CH_2 is investigated. Since no other relevant pathways for the formation of uracil and thymine were available in the literature, we consider a large gas-grain chemical network to study the chemical evolution of cytosine in gas and ice phases. Our modeling result shows that cytosine would be produced in cold, dense interstellar conditions. However, presence of cytosine is yet to be established. We propose that a new molecule, namely, $\text{C}_4\text{N}_3\text{OH}_5$ could be observable in the interstellar region. $\text{C}_4\text{N}_3\text{OH}_5$ is a precursor (Z isomer of cytosine) of cytosine and far more abundant than cytosine. We hope that observation of this precursor molecule would enable us to estimate the abundance of cytosine in interstellar regions. We also carry out quantum chemical calculations to find out the vibrational as well as rotational transitions of this precursor molecule along with three pyrimidine bases.

Subject headings: Astrochemistry; ISM: molecules; ISM: abundances; ISM: evolution; methods: numerical

1. Introduction

The process of origin of life is yet to be known with any certainty. Till date, it is a big puzzle even to explain the origin of complex organic and potentially pre-biotic molecules in the interstellar medium (ISM). As per the Cologne Database for Molecular Spectroscopy (CDMS catalog) (Muller et al. 2005, 2001), more than 190 molecules have been detected in the ISM or circumstellar shells and this number is increasing steadily. Complex molecules were detected in circumstellar envelopes, interstellar molecular clouds, interstellar ice, comets and meteorites. Examples of biologically important molecules detected in molecular clouds, range from the amino acetonitrile ($\text{NH}_2\text{CH}_2\text{CN}$) (Belloche et al. 2008) and proto-sugar glycolaldehyde (HOCH_2CHO) (Hollis et al. 2010) to possible pyrimidine and purine base precursor like HCN (Snyder & Buhl 1971), HNCO (Johansson et al. 1984), NCCCH (Ziurys 2006), HCONH_2 (Rubin et al. 1971).

Chakrabarti & Chakrabarti (2000a,b) computed abundances of several pre-biotic molecules including some bases of DNA and RNA during the collapse of proto-stellar clouds. They found that most of the molecules are formed in the gas phase even before the star or the planets are formed. Subsequently, Gupta et al. (2011); Merz et al. (2014) proposed other new reaction schemes for the formation of adenine in interstellar region. They computed the rate coefficients of these newly proposed reactions under interstellar circumstances. These complex bio-molecules could be synthesized both in gas and ice phases. Despite several observational supports, the complete chemical composition of ISM is yet to be determined with full confidence. In order to understand chemical composition of the ISM, it is required to model interstellar chemistry (gas and ice phase) by considering appropriate physical conditions. Recently, several authors (Das, Acharyya & Chakrabarti 2010; Das & Chakrabarti 2011; Das et al. 2013a,b; Majumdar et al. 2012, 2013, 2014a,b; Sahu et al. 2015; Cazaux et al. 2010; Chakrabarti et al. 2006a; Chakrabarti et al. 2006b

2006b; Das et al. 2008a,b; Cuppen et al. 2009) proposed to implement grain-surface chemistry to appropriately model the chemical processes. Considering a gas-grain chemical model, findings of Chakrabarti & Chakrabarti (2000a,b) have been revised with more accurate analysis by Das et al. (2013a) and Majumdar et al. (2012, 2013); Chakrabarti et al. (2015). Majumdar et al. (2012, 2013) found that trace amounts of bio-molecules (adenine, alanine, glycine etc.) could be produced during the collapsing phase of a proto-star. They suggested that observations of some of these precursor molecules could provide an educated guess about the abundances of these complex molecules under interstellar conditions.

Significant indications are now present that three important interstellar pyrimidine bases (cytosine, uracil and thymine) existed in the pre-biotic Earth (Wang & Bowie 2012). Despite high potential barriers, reactions among some interstellar molecules may lead to the formation of cytosine, uracil and thymine. A large number of experiments were carried out to explain formation of complex organic molecules in astrophysical environments. Most of these experiments mainly focused on the ultraviolet photo processing of low temperature ice mixture containing H_2O , CH_3OH , CO , CO_2 , NH_3 etc. and subsequent warming up (Bernstein et al. 1995; Muñoz & Schutte 2003). A wide variety of organic compounds were found by analysing residues. Nuevo et al. (2009); Nuevo, Milam & Sandford (2012); Nuevo, Materese & Sandford (2014) and Materese et al. (2013) found that the addition of pyrimidine to H_2O -rich binary mixtures which contain NH_3 , CH_3OH or CH_4 leads to the formation uracil, cytosine and thymine in presence of UV irradiation. These photo products were formed by successive addition of OH, NH_2 , and CH_3 groups to pyrimidine. Thymine was found to be produced only when UV dose was three times higher than that required to form cytosine and uracil. Nuevo, Materese & Sandford (2014) obtained trace amount of cytosine in their experiment. Low abundance of cytosine in comparison to the uracil was explained due to the low concentration of NH_3 in the initial ice mixture and/or conversion of cytosine into uracil via hydrolysis. Hydrolysis of cytosine for the formation

of uracil were also studied by Shapiro (1999) and Nelson et al. (2001). They claimed that the hydrolysis of cytosine is responsible for the non detection of cytosine in carbonaceous chondrites. Recently Gupta et al. (2013) attempted quantum chemical techniques to explore the possibility of cytosine formation in interstellar conditions. They proposed that some radical-radical and radical-molecular interactions could lead to the formation of interstellar cytosine. Despite overwhelmingly significant quantum chemical results, till date, any of these species have not been observed in the ISM. This motivates us to throw some lights on the status of three pyrimidine bases under interstellar circumstances.

Plan of this paper is the following. In Section 2, the computational details and construction of chemical model are discussed. Results are presented in Section 3, and finally, in Section 4, we draw our conclusions.

2. Methods and Computational Details

2.1. Chemical modeling

Our chemical model consists of a large gas-grain network where gas and grains are assumed to be interacting with each other continuously to exchange their chemical components.

For the simplicity, here we assume a static molecular cloud, with a constant density (n_H) and constant temperature (T). Since, we are considering a dense cloud condition, we assume that gas and grains are well coupled and have the same temperature (i. e., $T_{gas} = T_{grain} = T$). We adopt the initial elemental abundances (Table 1) by following Leung, Herbst & Huebner (1984). This kind of initial elemental abundances typical of the low-metal abundances has been adopted for TMC-1 (Das et al. 2015a).

Our present gas phase chemical network consists of 6349 reactions between 637 species

and surface chemical network consists of 305 reactions between 292 species. Various types of gas phase reactions are considered in the network, namely, ion (cation)-neutral, neutral-neutral, charge exchange, dissociative recombination, photo-dissociation, cosmic ray induced photo-dissociation, radiative association, associative detachment, radiative electron attachment and mutual neutralization. Except molecular hydrogen (according to Leitch-Devlin & Williams (1985), sticking coefficient of $\text{H}_2 \sim 0$ in low temperatures) and Helium (Roberts & Millar (2000) assumed that Helium would not stick to grains), depletion of all the gas phase neutral species onto the grain surface is considered with a sticking probability of unity.

2.2. Gas phase reaction network and rate coefficients

For the gas-phase chemical network, we follow UMIST 2006 database (Woodall et al. 2007). We considered the formation of various gas phase pre-biotic molecules following Majumdar et al. (2012, 2013); Chakrabarti et al. (2015). In this work, we also consider various neutral-neutral reactions, radical-molecular reactions (Gupta et al. 2013) for the formation of cytosine.

Gupta et al. (2013) use quantum chemical techniques to explore the possibility of cytosine formation by radical-radical and radical-molecule interaction schemes by barrier-less or low barrier pathways. They considered two different pathways (scheme 1 and scheme 2) for the formation of cytosine. In Table 2, we show all these pathways, where, reactions i-vii correspond to the scheme 1 and reactions viii-xiv correspond to the scheme 2 for the production of cytosine as mentioned in Gupta et al. (2013). For the formation of uracil from cytosine, we consider reaction xix, where reaction between water and cytosine were considered. For the synthesis of thymine from uracil, we consider reaction numbers xx, where the reaction with $:\text{CH}_2$ is considered. Here, for the simplicity and due to the

unavailability of the destruction reactions, we are not considering any destruction reactions either in the gas phase or in the ice phase and thus predicted abundances are only the upper limit.

Since exothermic and barrier-less reactions do not follow temperature-dependent Arrhenius expression, an estimate of rate coefficient at 30 K could be made on the basis of the semi-empirical relationship developed by Bates (1983):

$$k = \frac{1 \times 10^{-21} A_r (6E_0 + N - 2)^{3N-7}}{(3N - 7)!} \text{ cm}^3 \text{ s}^{-1}, \quad (1)$$

where, E_0 is the association energy in eV , A_r is the transition probability in s^{-1} (assumed to be 100), and N is the number of nuclei in the complex. A limiting rate is adopted if the calculated value exceeds the limit set by the following equation.

$$k = 7.41 \times 10^{-10} \alpha^{1/2} (10/\mu)^{1/2} \text{ cm}^3 \text{ s}^{-1}, \quad (2)$$

where, α is the polarizability in \AA^3 and μ is the reduced mass of the reactants on the ^{12}C *amu* scale.

Reactions, which are considered for the formation of cytosine are shown in Table 2 along with their gas phase rate coefficients at 10 K. All the reactions in the reaction network of cytosine (reactions i-xiv) are barrier-less except reaction iii. These reactions involve several simple neutral molecules and radicals such as HNCO (Bockelee-Morvan et al. 2000; Buhl et al. 1973; Nguyen et al. 1991), cyanoacetylene HCCCN (Bockelee-Morvan et al. 2000; Ziurys 2006; Coustenis et al. 1999), propynylidyne CCCH (Lucas et al. 1995), NH_2 (Van Dishoeck & Jansen 1993), NH (Wagenblast et al. 1993), OCN^- (Hudson & Moore 2000). Since reaction iii possesses a high activation barrier (52.30 kJ/mol, 1 kJ/mol= 120.274 K), this reaction is not feasible in the low temperature region.

Gupta et al. (2013) calculated activation barriers for these reactions but not the rate coefficients of these reactions. We used their activation barriers to compute rate coefficients

of these reactions by Eqn. 1. If the calculated rate exceeds the limiting rate ($\sim 10^{-9}$) set by Eqn. 2, we use the limiting rate only. For the computation of the limiting rate, we require to know the isotropic polarizability of the comparatively larger and stable reactant partner. This polarizability values were not available from Gupta et al. (2013). Polarizability of a species is defined as the second derivative of energy with respect to electric field, i.e., the first derivative of dipole moment with respect to the electric field. This defines the ability for a molecule to be polarized. The total isotropic mean molecular polarizability of a species is the mean value of polarizabilities in all three orthogonal directions. The polarizability tensor (is a 3×3 tensor) is said to be isotropic if its usual matrix representation is diagonal, with the three diagonal elements equal. For the computation of the isotropic polarizability, first we find out optimized geometry of the desired species and then by doing frequency calculation or polar calculation modeling on the optimized geometry, we find the isotropic polarizability. For this computation, we use the density functional theory based B3LYP functional with the 6-311++G** basis set of Gaussian 09 program.

We found that for the reactions ii, iv, v, vi, vii, x, xii and xiv, rate coefficients calculated by Eqn. 1 are crossing the limiting values. Comparatively larger and stable molecules in these reactions are C_3H_3N , $C_4N_3H_5O$, $C_4N_3H_6O$, $C_4N_3H_6O$, $C_4N_3H_6O$, $C_4N_2H_2O$, $C_4N_3H_4O$ and $C_4N_3H_6O$ for the reactions ii, iv, v, vi, vii, x, xii and xiv respectively. Our calculated isotropic polarizability of these species are found to be 6.94, 10.88, 11.31, 11.31, 11.31, 9.05, 11.37, 11.31 in the unit of \AA^3 for C_3H_3N , $C_4N_3H_5O$, $C_4N_3H_6O$, $C_4N_3H_6O$, $C_4N_3H_6O$, $C_4N_2H_2O$, $C_4N_3H_4O$ and $C_4N_3H_6O$ respectively.

Shapiro (1999); Nelson et al. (2001) proposed the hydrolysis of cytosine could form uracil (reaction xix). We investigate the usefulness of reaction xix under interstellar circumstances. Actually reaction xix is a two step process. First step is the water addition and 2nd step is the NH_3 elimination (Fig. 1). In the 1st step, water reacts with cytosine

Table 1: Initial abundances used relative to total hydrogen nuclei.

Species	Abundance
H ₂	5.00×10^{-01}
He	1.00×10^{-01}
N	2.14×10^{-05}
O	1.76×10^{-04}
H ₃ ⁺	1.00×10^{-11}
C ⁺	7.30×10^{-05}
S ⁺	8.00×10^{-08}
Si ⁺	8.00×10^{-09}
Fe ⁺	3.00×10^{-09}
Na ⁺	2.00×10^{-09}
Mg ⁺	7.00×10^{-09}
P ⁺	3.00×10^{-09}
Cl ⁺	4.00×10^{-09}
e ⁻	7.31×10^{-05}
HD	1.6×10^{-05}

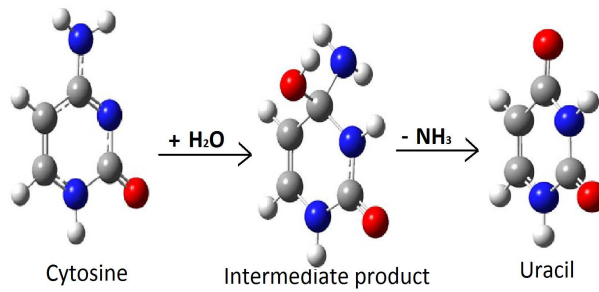


Fig. 1.— Uracil formation in two steps: 1st step is the addition of water with cytosine and 2nd step is the elimination of ammonia from the intermediate product.

to produce the 1st product. We compute the change of enthalpy (ΔH) for this step at B3LYP/6-311++G** level of theory. In gas phase, ΔH for the 1st step is 42.3123 kJ/mol. Thus it is highly endothermic in nature. We also calculate the activation barrier for the 1st step, which is 162.5 kJ/mol for the gas phase. These values are quite high in relation to the interstellar circumstances and the process is very unlikely to go through. In the cold interstellar clouds, averaged translational temperatures of the reactants are about 10 K, which can rise up to 4000 K in the outer photosphere of carbon stars (Kaiser et al. 1999). The transition state for the 1st step (gas phase) is shown in Fig. 2a.

In the 2nd step, there is an elimination of NH₃ from the intermediate product. We compute ΔH for this reaction at the same level of theory which comes out to be -83.788 kJ/mol for the gas phase. Thus, 2nd step is highly exothermic in gas phase. Activation barrier for this step comes out to be 117.76 kJ/mol for the gas phase. It is very interesting to note that despite highly exothermic nature of the 2nd step, it possesses very high activation energy barrier in the gas phase. It is very hard to overcome this energy barrier under interstellar condition. The transition state for the 2nd step is shown in Fig. 2b.

It is very clear from the above discussions that under the interstellar circumstances, formation of uracil from cytosine is not possible by the proposed reactions. Sklenak et al. (2004) also investigated the conversion of cytosine to uracil under deamination reaction catalyzed by yeast cytosine deaminase (a zinc metalloenzyme of sufficient biomedical interest) by using ONIOM method. Though their studies were not related to the interstellar scenario, it also shows that both the rate determining steps possess positive energy barriers. Wang & Bowie (2012) carried out some extensive ab-initio calculations to investigate the possibility of the formation of cytosine, uracil and thymine in interstellar regions. Various deamination reactions of cytosine were investigated by various authors but all these deamination reactions are indeed very slow in nature (Wang & Bowie (2012) and references

therein). For the formation of uracil, Wang & Bowie (2012) proposed a three body reaction between water, Urea and $:CCCO$ which is very unlikely to happen in interstellar condition. They also investigated the interconversion of uracil/cytosine by using neutrals, radicals and anions derived from ammonia. It is required to have minimum 108 kJ/mol energy for such interconversion. Thus, the chances of this interconversion are also limited.

We investigate thymine formation between uracil and $:CH_2$ (reaction xx) by following Wang & Bowie (2012). Transition state of this reaction is shown in Fig. 3. For this reaction, ΔH is -456.417 kJ/mol whereas the activation barrier is -84.96 kJ/mol. Our studies are in excellent agreement with the previous studies by Wang & Bowie (2012). For the computation of the gas phase rate coefficient of reaction xx, we use Eqn. 2. Polarizability of the largest reactant (uracil) we used is 9.85 \AA . Despite the low barrier energies of reaction xx, thymine would not be produced by this reaction. The reason behind is that uracil is required for reaction xx and uracil formation is limited by the high barriers of reaction xix. Thus the proposed gas phase pathways of Table 2 would only produce cytosine.

2.3. Surface reaction network and rate coefficients

It is now well established that grain chemistry plays a major role for the formation of complex molecules in interstellar region. Interstellar grain acts as a catalyst for the formation of complex interstellar molecules. In comparison with the dilute and tenuous interstellar gas, reaction probabilities on interstellar grains are enhanced by some orders of magnitudes. A detailed discussions on our gas-grain chemical model are already presented in Das, Acharyya & Chakrabarti (2010); Das & Chakrabarti (2011); Das et al. (2013a,b, 2015a,b,c); Majumdar et al. (2012, 2013, 2014a,b); Sivaraman et al. (2015).

Binding energies of the surface species mainly dictate chemical enrichment of interstellar

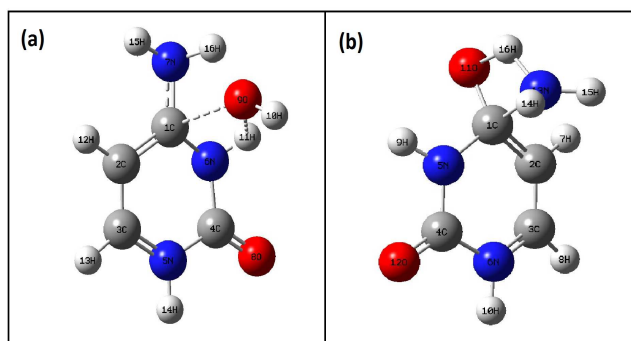


Fig. 2.— (a) Transition state of the 1st step, (b) Transition state of the 2nd step of reaction xix.

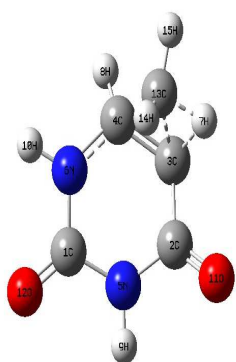


Fig. 3.— Transition state of reaction (xx).

Table 2: Reaction network along with its rate coefficients for the formation of three pyrimidine bases at $T = 10$ K

Species	Reaction pathways in gas/ice phase	Gas phase activation barriers in (kJ/mol)	Rate coefficients in gas phase ($\text{cm}^3 \text{s}^{-1}$) at 10 K	Rate coefficients in ice phase (s^{-1}) at 10 K
cytosine scheme 1	(i) $\text{HCCC} + \text{NH}_2 \rightarrow \text{C}_3\text{H}_3\text{N}$	-425.51^a	1.07×10^{-9c}	2.97×10^{-6e}
	(ii) $\text{C}_3\text{H}_3\text{N} + \text{NH} \rightarrow \text{C}_3\text{N}_2\text{H}_4$	-443.50^a	1.37×10^{-9d}	4.96×10^{-3e}
	(iii) $\text{C}_3\text{N}_2\text{H}_4 + \text{HNCO} \rightarrow \text{C}_4\text{N}_3\text{H}_5\text{O}$	52.30^a	–	–
	(iv) $\text{C}_4\text{N}_3\text{H}_5\text{O} + \text{H} \rightarrow \text{C}_4\text{N}_3\text{H}_6\text{O}$	-326.77^a	5.97×10^{-9d}	4.91×10^{1e}
	(v) $\text{C}_4\text{N}_3\text{H}_6\text{O} + \text{NH} \rightarrow \text{C}_4\text{H}_5\text{N}_3\text{O} + \text{NH}_2$	-249.37^a	1.67×10^{-9d}	4.96×10^{-3e}
	(vi) $\text{C}_4\text{N}_3\text{H}_6\text{O} + \text{OH} \rightarrow \text{C}_4\text{H}_5\text{N}_3\text{O} + \text{H}_2\text{O}$	-361.08^a	1.59×10^{-9d}	1.91×10^{-11e}
	(vii) $\text{C}_4\text{N}_3\text{H}_6\text{O} + \text{NH}_2 \rightarrow \text{C}_4\text{H}_5\text{N}_3\text{O} + \text{NH}_3$	-314.64^a	1.63×10^{-9d}	2.98×10^{-6e}
cytosine scheme 2	(viii) $\text{HCCCN} + \text{OCN}^- \rightarrow \text{C}_4\text{N}_2\text{OH}$	-83.68^a	1.94×10^{-16c}	7.92×10^{-14e}
	(ix) $\text{C}_4\text{N}_2\text{OH} + \text{H} \rightarrow \text{C}_4\text{N}_2\text{H}_2\text{O}$	-100.42^a	1.33×10^{-15c}	4.91×10^{1e}
	(x) $\text{C}_4\text{N}_2\text{H}_2\text{O} + \text{NH} \rightarrow \text{C}_4\text{N}_3\text{H}_3\text{O}$	-449.09^a	1.51×10^{-9d}	4.96×10^{-3e}
	(xi) $\text{C}_4\text{N}_3\text{H}_3\text{O} + \text{H} \rightarrow \text{C}_4\text{N}_3\text{H}_4\text{O}$	-248.11^a	6.42×10^{-10c}	4.91×10^{1e}
	(xii) $\text{C}_4\text{N}_3\text{H}_4\text{O} + \text{H} \rightarrow \text{C}_4\text{N}_3\text{OH}_5$	-304.60^a	6.11×10^{-9d}	4.91×10^{1e}
	(xiii) $\text{C}_4\text{N}_3\text{OH}_5 + \text{H} \rightarrow \text{C}_4\text{N}_3\text{H}_6\text{O}$	-157.32^a	6.6×10^{-13c}	4.91×10^{1e}
	(xiv) $\text{C}_4\text{N}_3\text{H}_6\text{O} + \text{H} \rightarrow \text{C}_4\text{H}_5\text{N}_3\text{O} + \text{H}_2$	-374.89^a	6.09×10^{-9d}	4.91×10^{1e}
	(xv) $\text{HNCO} + \text{H} \rightarrow \text{HNCHO}$	–	–	4.91×10^{1e}
	(xvi) $\text{HNCO} + \text{H} \rightarrow \text{NH}_2\text{CO}$	–	–	4.91×10^{1e}
	(xvii) $\text{HNCO} + \text{NH}_3 \rightarrow \text{OCN}^- + \text{NH}_4^+$	–	–	8.82×10^{-10e}
(xviii) $\text{HNCO} + \text{H}_2\text{O} \rightarrow \text{OCN}^- + \text{H}_3\text{O}^+$	–	–	9.04×10^{-14e}	
Uracil	(xix) $\text{C}_4\text{H}_5\text{N}_3\text{O} + \text{H}_2\text{O} \rightarrow \text{Reaction intermediate}$	162.5^b	–	–
	Reaction intermediate $\rightarrow \text{C}_4\text{H}_4\text{N}_2\text{O}_2 + \text{NH}_3$	117.76^b	–	–
Thymine	(xx) $\text{C}_4\text{H}_4\text{N}_2\text{O}_2 + \text{CH}_2 \rightarrow \text{C}_5\text{H}_6\text{N}_2\text{O}_2$	-84.96^b	1.61×10^{-9d}	1.67×10^{-7e}

^a Gupta et al. (2013)

^b Present work

^c Calculated by Eqn. 1

^d Calculated by Eqn. 2

^e Calculated by Eqn. 3

grain mantle. Required desorption energies (E_d) for this calculations are mainly taken from Allen & Robinson (1977), Hasegawa & Herbst (1993). Following Hasegawa, Herbst & Leung (1992), here also, we assume that the binding energy against diffusion (E_b) = $0.3E_d$ except the case of atomic hydrogen. Similar to Hasegawa, Herbst & Leung (1992), here also we use, $E_b = 100$ K for atomic hydrogen. Desorption energy of HNCO is considered to be 1425 K (Garrod, Weaver & Herbst 2008). Since desorption energy of HNHCO, NH₂CO, OCN⁻, NH₄⁺, H₃O⁺ were unavailable, we choose their desorption energies to be 1425 K, same as HNCO, so that all their binding energies are $E_b = 0.3E_d \sim 427.5$ K. For the larger species, such as C₄N₂HO, C₄N₂H₂O, C₄N₃H₃O, C₄N₃H₄O, C₄N₃OH₅ & C₄N₃H₆O, we set the desorption energy to 5000 K. Rate coefficient of the ice phase reactions are calculated by the following relation (Hasegawa, Herbst & Leung 1992),

$$R = k_{ab}(R_a + R_b)N_aN_bn_d, \quad (3)$$

where, N_a and N_b are the number of a and b species on an average grain respectively, k_{ab} is the probability for the reaction to happen upon an encounter and n_d is dust-grain number density, R_a and R_b are the diffusion rates, for species a and b respectively. Diffusion rate ($R_a = N_s t_a$ and $R_b = N_s t_b$) depends on the time required to traverse the entire grain by the reactive species, which in turn depends on

$$t_a = 1/\nu_0 \exp(E_b/kT_g) \text{sec},$$

where ν_0 is the characteristic vibration frequency of the adsorbed species, E_b is the binding energy, T_g is the grain temperature and N_s is the number of surface sites on a grain. For the computation of the characteristic vibration frequency (ν_0), we utilize the following harmonic oscillator relation:

$$\nu_0 = \sqrt{2n_s E_d / \pi^2 m},$$

where, n_s is the surface density and m is the mass of the species. As in our previous model, here also, we use $N_s = 10^6$ and $n_s = 2 \times 10^{14} \text{ cm}^{-2}$ (Das et al. 2015a).

Various types of evaporation mechanisms are considered here, namely, thermal desorption, cosmic ray induced desorption and non-thermal desorption. Thermal desorption time scale depends on the desorption energy of the species by following the relation (Hasegawa, Herbst & Leung 1992):

$$t_{thermal} = \nu_0^{-1} \exp(E_d/KT_g) \text{ sec}^{-1}.$$

Cosmic ray induced desorption time scale follows from the relation described by Hasegawa & Herbst (1993),

$$t_{crd} = t_{thermal}/f(70, K),$$

where, $f(70, K) = 3.16 \times 10^{-19}$. Garrod, Wakelam & Herbst (2007) estimated non-thermal desorption rate via exothermic surface reactions by considering Rice-Ramsperger-Kessel (RRK) theory. They parameterized non-thermal desorption by assuming certain approximations. They assumed that a fraction f of the product species in qualifying reactions could desorb immediately and the rest $(1-f)$ fraction remains as a surface bound product. Here, we apply this mechanism to all surface reactions which result in a single product. Fraction f is calculated by;

$$f = \frac{aP}{1 + aP},$$

where, a is the ratio between surface molecule bond frequency to frequency at which energy is lost to grain surface. Here, as in Garrod, Wakelam & Herbst (2007), we consider a moderate value of a (i.e., $a = 0.012$) for our simulation.

Gupta et al. (2013) carried out quantum chemical calculations (using PCM model) for the formation of cytosine in ice phase as well. Their calculations shows that similar to the gas phase reactions, only reaction iii of scheme 1 is having positive activation barrier. Rest of the reactions are barrier-less in ice also. Here, in our model, we are considering these reactions in ice phase also. Rate coefficients for these reactions in ice phase are computed by using eqn. 3. All the ice phase rate coefficients are shown in Table 2 at 10 K.

For the production of cytosine via scheme 2, OCN^- is essential. The $4.62 \mu\text{m}/2165 \text{ cm}^{-1}$ feature is very often attributed to the solid state OCN^- (Soifer et al. 1979; Mispelaer et al. 2012; Grim et al. 1987). Mispelaer et al. (2012) carried out an investigation to study the formation of OCN^- by reaction xvii (reaction between HNCO & NH_3). According to their study, this reaction would follow Arrhenius law with an activation energy of $0.4 \pm 0.1 \text{ kJ/mol}$ ($48 \pm 12 \text{ K}$) with a pre-exponential factor of $0.0035 \pm 0.0015 \text{ s}^{-1}$. The proposed reaction would favourably produce OCN^- if it occurs in the NH_3 rich (excess with respect to HNCO) environment. In the ice phase, NH_3 would be mainly produced by the hydrogenation of nitrogen. For the formation of HNCO , we are not considering any ice phase reactions. In our gas phase network, HNCO would be produced by the reactions mentioned in McElroy et al. (2013). Since, we are considering gas-grain interactions, our ice phase would be populated by gas phase HNCO . Mispelaer et al. (2012) showed that reaction xvii occurs in two steps. First step is a slow process having typical rate coefficient of $k_o = 4.9 \times 10^{-6} \text{ s}^{-1}$ at 10 K and second step is relatively faster having rate coefficient of $k_r = 1.8 \times 10^{-4} \text{ s}^{-1}$ at 10 K. Thus overall rate of this reaction at 10 K is $k = k_o k_r = 8.82 \times 10^{-10} \text{ s}^{-1}$. In our simulation, we are also considering this rate coefficient for reaction xvii at 10K. If the rate coefficient of reaction xvii is calculated by eqn. 3, then it would become $1.61 \times 10^{-9} \text{ s}^{-1}$. Thus, proposed rate coefficient by Mispelaer et al. (2012) is 1.8 times slower than the rate coefficient calculated by thermal hopping mechanism (eqn. 3). Reaction number xviii may also contribute to the formation of OCN^- (van Broekhuizen et al. 2004). The rate coefficient of this reaction is calculated by eqn. 3 and the value of this rate coefficient is $9.04 \times 10^{-14} \text{ s}^{-1}$. It is roughly 4 orders lower than the rate coefficient of reaction xvii. Thus OCN^- is mainly produced by reaction xvii.

We carry out quantum chemical calculations to check the possibility of formation of uracil (reaction xix) and formation of thymine (reaction xx) in ice phase also.

For studying grain surface reactions i.e., reactions in astrophysical ice, one needs to incorporate bulk passive influence of water. We modelled this effect by considering a self-consistent reaction field in the electronic structure calculations under Gaussian 09 program. Here the reaction components are subject to polarization effects due to the collective static electric field arising from the large dipole and higher moments of the bulk water matrix. Water changes the energetic of chemical reactions in both active and passive ways. Water molecules may actively serve as a catalyst, facilitating proton transfer or other behaviour in chemical reactions. The reaction components are also subject to polarization effects due to the collective static electric field arising from the large dipole and higher moments of the bulk water matrix. This is a passive influence that can also change the barrier heights of reactions that occur within the ice matrix. So depending on the active and passive influence of water, pathways, barrier as well as rates can differ. To study reaction kinetics of the formation of uracil and thymine from cytosine in ice phase, we use density functional theory based B3LYP functional with the 6-311++G** basis set using Gaussian 09 program. We adopt Self Consistent Reaction Field (SCRF) modeling using the polarizable continuum model (PCM) with the integral equation formalism variant (IEFPCM) as the default SCRF method. This method in Gaussian 09 program is used to include the bulk solvation effect of the interstellar grain mantle (mostly water ice). For the SCRF modeling, bulk solvent medium is simulated as a continuum of the dielectric constant (for water =78.5) which surrounds a solute cavity, defined by the union of a series of interlocking spheres centered on the reactive atoms.

As like the gas phase (Fig. 1), reaction xix would process in two steps. ΔH for the first step of this reaction is 76.27 kJ/mol and for the second step is -95.23 kJ/mol. Thus, first step of reaction xix is endothermic whereas the second step is exothermic in ice phase. Activation barriers for these two steps are 163.05 kJ/mol and 108.87 kJ/mol in the ice phase. Due to these high barrier energies, reaction xix would not able to process in

ice phase as well. Thus formation of uracil in ice phase is not possible. For the thymine formation (reaction number xx) in ice phase, reaction of uracil with :CH_2 is studied. ΔH for this reaction -415.59 kJ/mol in ice phase. Thus this reaction is exothermic in nature. Activation barriers for this reaction is -65.48 kJ/mol. Since the activation barrier for reaction between uracil and :CH_2 (reaction xx) is favourable under interstellar condition, this reaction would process in interstellar ice. Now, reaction xx require uracil for the production of thymine. Since uracil is not forming on the ice, production of thymine on the interstellar ice is questionable. Thus, we are not considering reaction numbers xix-xx in our surface chemical network. Rate coefficient for reaction xx in ice phase is shown in Table 2 for the illustration purpose.

3. Results and Discussion

3.1. Modeling results

In Fig. 4, we show chemical evolution of cytosine in gas phase and ice phase. ‘Y’ axis of Fig. 4 represents logarithmic abundance of species (n_x) with respect to number density of total hydrogen nuclei in all forms (n_H). To mimic dense interstellar conditions, we consider an intermediate dense cloud ($n_H = 10^5 \text{ cm}^{-3}$) having $T = 10$ K and $A_V = 10$. OCN^- is the basic requirement for the formation of cytosine and it is producing efficiently on the ice phase. Due to the moderate desorption energy of OCN^- , it is populating the gas phase to process cytosine formation in gas phase as well.

It is evident from Fig. 4 that the abundance of cytosine is beyond the present observational limit (Agu n dez & Wakelam 2013). Thus it would be more helpful, if we identify an intermediate molecule as the precursor of cytosine. Here, we consider $\text{C}_4\text{N}_3\text{OH}_5$ (Z isomer of cytosine) as the precursor (Fig. 5a). Gupta et al. (2013) obtained this structure

during the synthesis of cytosine starting from OCN^- and HCCCN . There is another isomer of cytosine (i.e., E isomer) which would also be formed starting from OCN^- and HCCCN . Structure of the E isomer of cytosine is shown in Fig. 5b. Though the E isomer is more stable than the Z isomer (optimization energy of the Z isomer is 6.8 kJ/mol higher than the E isomer), we are considering the Z isomer only because the pathways with this isomer are available for the formation of cytosine. We also check the most economic route for the formation of cytosine starting from the precursor (Z or E isomer of cytosine). We compare ΔH of reaction (xiii), where, $\text{C}_4\text{N}_3\text{H}_6\text{O}$ is forming by the reaction between the precursor (Z or E isomer) and H atom. ΔH for the reaction between H atom and Z isomer is -155.914 kJ/mol and between H atom and E isomer is -154.07 kJ/mol. Thus reaction with the Z isomer is more endothermic than the reaction with the E isomer towards the final step of the cytosine production. In Fig. 4, time evolution of $\text{C}_4\text{N}_3\text{OH}_5$ is also shown. It is clear that it could efficiently be produced. Peak abundance of gas phase cytosine and $\text{C}_4\text{N}_3\text{OH}_5$ is found to be 1.06×10^{-16} , 6.36×10^{-16} respectively and for the ice phase it is found to be 3.72×10^{-16} , 4.44×10^{-14} respectively. It is expected that all the ice phase species would populate the gas phase during the warm up phase of a collapsing cloud. Thus the ice phase abundance of the precursor molecule would be reflected in the gas phase as well.

3.2. Astronomical Spectroscopy

3.2.1. Vibrational transitions

Gas phase vibrational frequencies of three pyrimidine bases and one of their precursor ($\text{C}_4\text{N}_3\text{OH}_5$) are shown in Fig. 6. For these calculations, we use B3LYP/6-311G++(d,p) level of theory in Gaussian 09 program. Three most distinct peaks of cytosine appear at 1768, 1680 and 1632 cm^{-1} respectively. In case of uracil, two peaks are very strong, which are at 1800 and 1768 cm^{-1} . In case of thymine, two strongest peaks appear at 1800 and

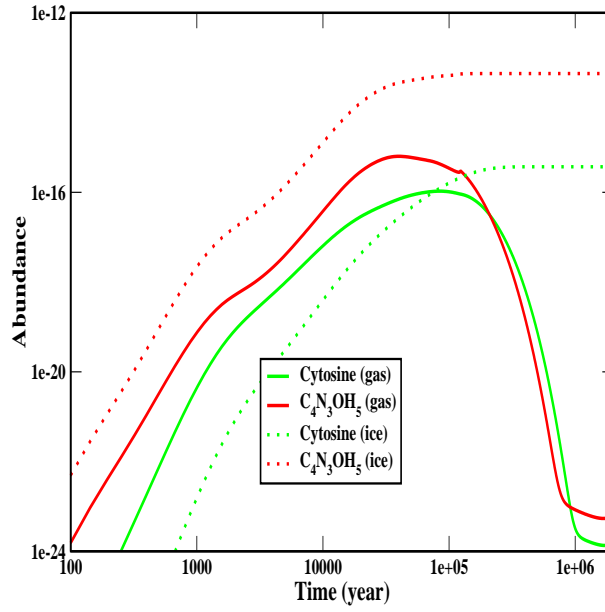


Fig. 4.— Chemical evolution of cytosine along with its precursor ($C_4N_3OH_5$).

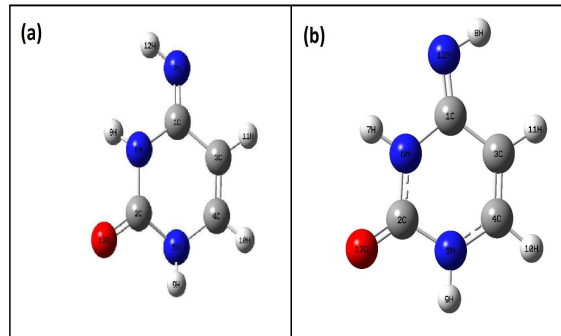


Fig. 5.— Structure of (a) Z isomer and (b) E isomer of $C_4N_3OH_5$.

1752 cm^{-1} . In case of the precursor molecule ($\text{C}_4\text{N}_3\text{OH}_5$), two strong peaks appear at 2359 and 1792 cm^{-1} . For a better illustration, we show the peak positions along with the band assignments of these species in Table A1. In Table A1, we compared our calculated vibrational frequencies with the earlier existing experimental works to justify the accuracy of our calculations. It is true that the validity of the band assignments are not obvious because there are some earlier works which reported the similar issues. But to the best of our knowledge, there are no such information available for $\text{C}_4\text{N}_3\text{OH}_5$. For the sake of completeness and to validate the accuracy of our results on $\text{C}_4\text{N}_3\text{OH}_5$, we summarize the vibrational frequencies and band assignments of cytosine, uracil and thymine along with $\text{C}_4\text{N}_3\text{OH}_5$.

3.2.2. Rotational transitions

In Table 3, rotational constants of three pyrimidine bases along with one precursor are shown. It is now well known that density functional theory can be applied to various astrophysical problems with sufficient accuracy (Runge & Gross 1984; Puletti et al. 2010; Pieve et al. 2014). Accuracy of the computed spectroscopic constant depends on the choices of the models. For example, Carles et al. (2013, 2014) fitted the experimental rotational frequencies to obtain spectroscopic constants and compared it with the theoretical quantum chemical calculations at the B3LYP/cc-pVTZ level of theory using Gaussian 09 program. Their results are in excellent agreement with the theory. Here also, we used the B3LYP/cc-pVTZ level of theory for the computation. It is clear from Table 3 that our calculated rotational constants (B and C) are in very good agreement with the experimentally measured values in experiments. But experimentally measured value of A deviates more from our calculated value. This difference could be attributed due to the difference between the techniques involved. Calculation of rotational constants refer to

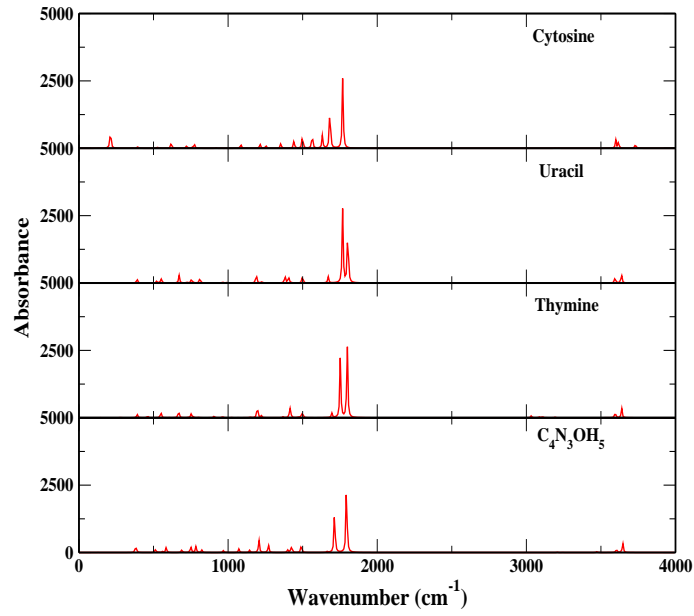


Fig. 6.— Infrared spectra of three pyrimidine bases and their precursor in gas phase.

an equilibrium geometry, while the measured ones are subject to some vibrational effects also (Csazar 1989). Experimentally extracted values might contain some uncertainties. Uncertainty is basically the expected errors of the experimental frequencies which are based on the propagation of errors estimated from a least squares fit of the observed frequencies to a model Hamiltonian. These predicted uncertainties of transition frequencies are strongly model dependent. Predicted uncertainties are smaller if large number of transition frequencies are measured and then implemented in the fit. Gaussian 09 program generate these parameters from the computation of anharmonic frequencies and analytic second derivative of energies at displaced geometries. These analytic computations are highly accurate and thus they does not reflect any uncertainties in their results. Some earlier theoretical/experimental works have been performed to find out the rotational constants of cytosine and uracil. Here, we also use the B3LYP/cc-pVTZ level of theory in Gaussian 09 program for the computation. In Table 3, we compare our results with the existing results. It is clear from the table that our calculated values are in good agreement with the earlier results.

These rotational constants are used in SPCAT program (Pickett 1991) to generate several rotational transitions. These transitions are used in ASCP program (Kisiel et al. 1998, 2000) for the representation of the rotational stick diagram (Fig. 7) at 300 K.

4. Concluding Remarks

In this paper, we explored the possibility of formation of three pyrimidine bases, namely, cytosine, uracil and thymine in interstellar region. We studied the hydrolysis of cytosine for the formation of uracil. Our results strongly suspects the validity of this reaction around the low temperature regime. Since uracil production is limited by the hydrolysis reaction, production of thymine by the reaction between uracil and CH_2 is highly

Table 3: Rotational constants for cytosine, uracil, thymine and one of its precursor at B3LYP/cc-pVTZ level of theory

Species	Parameter	Values (in MHz)	Experimental/observational results
Cytosine	<i>A</i>	3846.1573	3871.54618 ^d
	<i>B</i>	2012.0252	2024.97804 ^d
	<i>C</i>	1321.6224	1330.33627 ^d
Uracil	<i>A</i>	3902.4459	3883.873021 ^a , 3883.87825 ^b , 3902.4 ^c
	<i>B</i>	2022.1182	2023.732581 ^a , 2023.73267 ^b , 2022.2 ^c
	<i>C</i>	1331.9473	1330.928108 ^a , 1330.92380 ^b , 1332.0
Thymine	<i>A</i>	3212.0066	3201.20 ^e
	<i>B</i>	1404.9181	1401.81 ^e
	<i>C</i>	9832.6168	9826.1 ^e
C ₄ N ₃ OH ₅	<i>A</i>	3881.84	-
	<i>B</i>	2011.83	
	<i>C</i>	1325.08	
^a Experimental values by Brunken et al. (2006) ^b Experimental values by Brown et al. (1988) ^c Calculated values by Brunken et al. (2006) at B3LYP/cc-pVTZ level of theory ^d Calculated values by Alonso et al. (2013) at MP2/6-311++G(d,p) level of ^e Experimental values by Brown et al. (1989)			

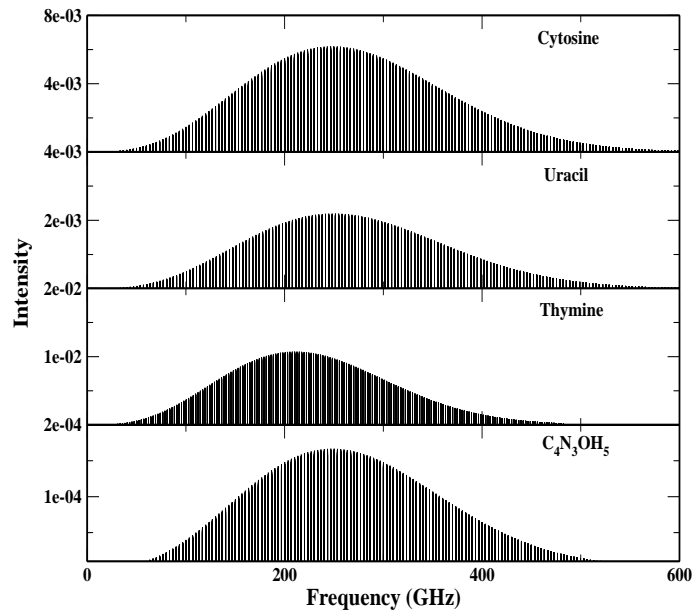


Fig. 7.— Rotational stick diagram of three pyrimidine bases and their precursor.

unlikely. However, the formation of cytosine is energetically favourable (in gas and ice phase) and thus we consider cytosine formation reactions in our gas-grain chemical model. Our calculated abundance suggests that trace amount of cytosine could be produced in the interstellar circumstances. Since, we are not considering any destruction reactions of cytosine, our predicted value merely reflects its upper limit. Despite this, our calculated abundance of cytosine is below the observational limit. This prompted us to propose to observe one precursor molecule of cytosine (intermediate product of cytosine route) whose abundance is much greater than cytosine. $C_4N_3OH_5$ could be used as the precursor molecule of cytosine. It is not obvious that the cytosine is harder to detect as compare to $C_4N_3OH_5$ based on the abundance argument only. Das et al. (2015a,b) already discussed this issue in detail and also mentioned the necessity of chemical modeling coupled with spectroscopic calculations prior to any astronomical survey. Our computed rotational spectroscopic data, abundances could used for radiative transfer modeling. It is now well known how the results of radiative transfer modeling play a crucial role for observing any species in the ISM (Coutens et al. 2014). Moreover, we carried out quantum chemical calculations to represent vibrational transitions of three pyrimidine bases along with the precursor of cytosine. Band assignments and a comparison with the earlier works have been carried out. Rotational constants of these bio-molecules are also computed by quantum chemical calculations and rotational stick diagrams are presented for the illustration purposes.

5. Acknowledgment

AD, SKC, & PG thank ISRO respond project (Grant No. ISRO / RES / 2/ 372/ 11-12) and DST project (Grant No. SB/S2/HEP-021/2013) for partial supports. LM thanks MOES and ERC starting grant (3DICE, grant agreement 336474) for funding during this work. We thank Mr. R. Saha for his help in data reduction.

REFERENCES

- Aguídez, M., Wakelam, V., 2013, *Chemical Reviews*, 113, 8710
- Alonso, J. L., Vaquero, V., Pea, I., Lopez, J. C., Mata, S., Caminati, W., 2013, *Angew. Chem. Int. Ed.*, 52, 2331
- Allen, M., Robinson, G. W., 1977., *ApJ*, 212, 396
- Bates, D. R. 1983, *ApJ*, 270, 564
- Bernstein, M. P., Sandford, S. A., Allamandola, L. J., et al. 1995, *ApJ*, 454, 327
- Muñoz Caro, G. M., & Schutte, W. A. 2003, *A&A*, 412, 121
- Belloche, A., Menten, K. M., Comito, C., Muller, H. S. P., Schilke, P., Ott, J., Thorwirth, S., Hieret, C., 2008, *A & A*, 482, 179
- Bockelee-Morvan, D., Lis, C., Wink, J.E., Despois, D., et al., 2000, *A&A*, 353, 1101
- van Broekhuizen, F. A., Keane, J. V., Schutte, W. A., 2004, *A&A*, 415, 425
- Brunken, S., McCarthy, M. C., Thaddeus, P., Godfrey, P. D., Brown, R. D., 2006, *A&A*, 459, 317
- Brown, R. D., Godfrey, P., McNaughton, D., Pierlot, A. P. 1988, *J. Am. Chem. Soc.*, 110, 2329
- Brown, R. D., Godfrey, P., McNaughton, D., Pierlot, A. P. 1989, *J. Chem. Soc., Chem. Commun.*, 1, 37
- Buhl, D., Snyder, L.E., Schwartz, P.R., Edrich, J., 1973, *Nature*, 243, 513.
- Carles, S., Møllendal, H. , and Guillemin, J.-C., 2013, *A&A*, 558, A6

- Carles, S., Mollendal, H., Trolez, Y., Guillemin, J, C, 2014, A&A, 564, 82
- Csaszar, A., G., Chemical Physics Letter, 1989, 162, 4
- Cazaux, S., Cobut, V., Marseille, M., Spaans, M., Caselli, P. 2010, A&A,522, 74
- Chakrabarti, S.K., Majumdar, L., Das, A., Chakrabarti, S., 2015, Astrophysics Space Science, 357,90
- Chakrabarti, S.K., Chakrabarti, S., 2000, A&A, 354, L6
- Chakrabarti, S.K., Chakrabarti, S., 2000, Ind. J. Phys., 74B, 97
- Chakrabarti, S.K., Das, A., Acharyya, K., Chakrabarti, S., 2006, A&A, 457, 167
- Chakrabarti, S.K., Das, A., Acharyya, K., Chakrabarti, S., 2006, BASI, 34, 299
- Coustenis, A., Schmitt, B., Khanna, R.K., Trotta, F.,1999, Planet. Space Sci., 47, 1305
- Coutens, A. et al., 2014, MNRAS, 445, 1299
- Colarusso, P., Zhang, K., Guo, B., Bernath, P., 1997, Chem. Phys. Lett., 269, 39
- Cuppen, H. M., Van Dishoeck E., F., Herbst, E., Tielens, A. G. G. M., 2009, A&A, 508, 275
- Das, A., Chakrabarti, S. K., Acharyya K. & Chakrabarti, S., 2008a, NEWA, 13, 457
- Das, A., Acharyya, K., Chakrabarti, S. & Chakrabarti, S. K.,2008b, A & A, 486, 209
- Das, A., Acharyya, K. & Chakrabarti, S. K., 2010, MNRAS 409, 789
- Das, A. & Chakrabarti, S. K., 2011, 418. 545, MNRAS
- Das, A. Majumdar, L., Chakrabarti, S. K., & Chakrabarti S., 2013a, New Astronomy, 23,

- Das, A. Majumdar, L., Chakrabarti, S. K., Saha, R., Chakrabarti S., 2013b, MNRAS, 433, 3152
- Das, A. Majumdar, L., Chakrabarti, S. K., Sahu, D., 2015a, New Astron., 35, 53
- Das, A. Majumdar, L., Sahu, D., Gorai, P., Sivaraman, B., Chakrabarti, S. K., 2015b, ApJ, 808, 21
- Das, A. Majumdar, L., Sahu, D., Chakrabarti, S. K., 2015c, MNRAS, eprint arXiv:1510.00117
- Garrod, R.T., Wakelam, V., Herbst, E., 2007. A&A 467, 1103
- Garrod, R.T., Wakelam, V., Herbst, E., 2008. ApJ, 682, 283
- Graindourze, M., Smets, J., Zeegers-Huyskens, T., Maes, G., J. Mol. Structure, 1990, 222, 345
- Grim, R. J. A., & Greenberg, J. M. 1987, ApJ, 321, L91
- Gupta, V. P, Tandon, P., Mishra, P., 2013, Adv. Space Res., 51, 797
- Gupta, V.R., Tandon, P., Rawat, P., Singh, R.N., Singh, A., 2011. A&A 528, A129.
- Hasegawa T., Herbst E., 1993, MNRAS, 261, 83
- Hasegawa, T., Herbst, E., Leung, C.M., 1992, APJ, 82, 167
- Hollis, J. M., Lovas, F. J., Jewell, P. R., 2000, APJ, 540, L107.
- Hudson, R.L., Moore, M.H., 2004, ICARUS 172, 466, 2004
- Johansson, L. E. B., Andersson, C., Ellder, J., Friberg, P., Hjalmarson, A., Høglund, B., Irvine, W. M., Olofsson, H., Rydbeck, G., 1984, A& A,130, 227

- kaiser, R. I., Ochsenfeld, C., Head-Gordon, M., Lee, Y. T., 1999, APJ, 510, 784
- Kisiel, Z., Biakowska-J. E., , Pszczkowski L., 1998, J. Chem. Phys., 109, 10263
- Kisiel, Z., Biakowska-J. E., , Pszczkowski L., 2000, J. Mol. Spectrosc., 199, 5
- Kwiatkowski, J. S., Leszczynski, J., 1996, J. Phys. Chem., 100, 941
- Leitch-Devlin, M., A., Williams, D., A., 213, 295, MNRAS, 1985
- Leung, C.M., Herbst, E., Huebner, W.F., 1984. ApJ 56, 231
- Lés, A., Adamowicz, L., Nowak, M. J., Lapinski, L., 1992, Spectrochimica Acta, 48, 1385
- Lucas, R., Guelin, M., Kahane, C., Audinos, P., Cernicharo, J., 1995 APSS, 224, 293
- Majumdar, L., Das, A., Chakrabarti, S.K., Chakrabarti, S., 2014a, A&A, 562, A56
- Majumdar, L., Das, A., Chakrabarti, S.K., Chakrabarti, S., 2014b, ApJ, 782, 73
- Majumdar, L., Das, A., Chakrabarti, S.K., Chakrabarti, S., 2013, New Astronomy, 20, 15
- Majumdar, L., Das, A., Chakrabarti, S.K., Chakrabarti, S., 2012, Research in Astronomy
& Astrophysics, 12, 1613
- McElroy, D., Walsh, C., Markwick, A. J., Cordiner, M. A., Smith, K., Millar, T. J., 2013,
A&A, 550, A36
- Mispelaer, F., Theule, P., Duvernay, F., Roubin, P., Chiavassa, T., 2012, A&A, 540, A40
- Merz, K. M., Aguiar, E. C., da Silva, J. B., 2014, JPhCA, 118, 3637
- Muller, H. S. P., Schloder, F., Stutzki, J., Winnewisser, G., 2005, JMoSt, 742, 215
- Muller, H. S. P., Thorwirth, S., Roth, D. A., Winnewisser, G., 2001, A&A, 370, L49

- Materese, C. K., Nuevo, M., Bera, P. P., et al. 2013, *AsBio*, 13, 948
- Nguyen-Q-Rieu, Henkel, C., Jackson, J.M., Mauersberger, 1991, *A&A*, 241, L33
- Nuevo, M., Milam, S. N., & Sandford, S. A. 2012, *AsBio*, 12, 295
- Nuevo, M., Milam, S. N., Sandford, S. A., et al. 2009, *AsBio*, 9, 683
- Nuevo, M., Materese, C. K., Sandford, S. A., et al. 2009, *AsBio*, 9, 683
- Nelson, K. E., Robertson, M. P., Levy, M., & Miller, S. L. 2001, *OLEB*, 31, 221
- Pickett, H.M., 1991, *J. Mol. Spectrosc.* 148, 371.
- Pieve, F. Da, Avendano-Franco, G., Proft, F. De, Geerlings, P., 2014, *MNRAS*, 440,494
- Puletti F., Mallocci G., Mulas G., Cecchi-Pestellini C., 2010, *MNRAS*, 402,1667
- Roberts, H., Millar, T. J., 2000, *A&A*, 361, 388
- Rubin, R. H., Swenson, G. W., Bensen, R. C., Tigelaar, H. L., and Flygare, W. H., 1971, *APJ*, 169, L39.
- Runge, E., Gross, E. K. U., 1984, *Phys. Rev. Lett.*, 52, 997
- Sahu, D., Das, A., Majumdar, L., Chakrabarti, S. K., 2015, *New Astron.*, 38, 23
- Soifer, B. T., Puetter, R. C., Russell, R. W., et al. 1979, *ApJ*, 232, L53
- Sivaraman, B., Radhika, N., Das, A., et al. 2015, 448, 1372
- Shapiro, R. 1999, *PNAS*, 96, 4396
- Snyder, L.E., Buhl, D., 1971, *APJ*, 163, L47
- Sklenak, S., Yao, L., Cukier, R. I., Yan, H., 2004, *J. Am. Chem. Soc.*, 126, 14879

Van Dishoeck, E.F., Jansen, D.J., 1993, *ApJ*, 416, L83

Wagenblast, R., Williams, D.A., Millar, T.J., Nejad, L.A.M., 1993, *MNRAS Lett.*, 260 (2),
420

Woodall, J., Agnèz, M., Markwick-Kemper, A.J., Millar, T.J., 2007, *A&A*, 466, 1197

Wang, T., Bowie, J. H., 2012, *Org. Biomol. Chem.*, 10, 652

Ivanov, A. Y., Plokhotnichenko, A. M., Radchenko, E. D., Sheina G. G., Blagoi, Y. P., 1995
J. Mol. Struct., 372, 91.

Ziurys, L. M., 2006, *Proc. Natl. Acad. Sci. U. S. A.*, 103, 12274

TABLE A1

VIBRATIONAL FREQUENCIES OF CYTOSINE, URACIL, THYMINE and C₄N₃OH₅ IN GAS PHASE AT B3LYP

6-311g++(D,P) LEVEL OF THEORY

Species	Peak positions (Gas phase) (in cm ⁻¹)	Integral absorption coefficient in (cm molecule ⁻¹)	Band assignments	Experimental/ calculated values (in cm ⁻¹)
Cytosine	128.49	3.33×10 ⁻¹⁹	skeletal deformation	270 ^e , 235 ^f
	196.35	1.27×10 ⁻¹⁸	NH ₂ bending out of plane	291 ^f
	211.91	3.85×10 ⁻¹⁸	NH ₂ bending	305 ^f
	358.27	5.16×10 ⁻¹⁹	NH ₂ bending	558.6 ^e , 550 ^f
	395.08	3.44×10 ⁻¹⁸	NCC bending	397 ^e , 400 ^f
	524.64	2.02×10 ⁻¹⁸	NH ₂ twisting	531 ^e , 535 ^f
	532.99	4.16×10 ⁻¹⁹	skeletal deformation	531 ^e , 535 ^f
	545.16	4.58×10 ⁻¹⁹	skeletal deformation	531 ^e , 535 ^f
	578.70	4.22×10 ⁻¹⁹	skeletal deformation	571 ^e , 575 ^f
	618.98	1.10×10 ⁻¹⁷	NH bending	614 ^e , 614 ^f
	722.56	4.95×10 ⁻¹⁸	CH bending	717 ^e , 716 ^f
	762.36	1.54×10 ⁻¹⁸	skeletal deformation	749 ^e , 747 ^f
	765.66	7.65×10 ⁻¹⁹	ring deformation	767 ^e , 747 ^f
	773.85	7.65×10 ⁻¹⁸	NCN bending out of plane	784 ^e , 818 ^f
	919.63	7.47×10 ⁻¹⁹	NC stretching	2922 ^e , 2930 ^f
	956.98	1.09×10 ⁻¹⁹	CH bending	
	986.25	7.60×10 ⁻²⁰	CC stretching	
	1085.37	7.97×10 ⁻¹⁸	NH ₂ rocking	1088 ^f
	1125.37	5.55×10 ⁻¹⁹	CH bending	1103 ^e , 1090 ^f

	1214.06	8.21×10^{-18}	<i>CH</i> wagging	1198 ^e , 1196 ^f
	1253.75	5.01×10^{-18}	<i>NC</i> stretching	1237 ^e , 1244 ^f
	1353.84	9.42×10^{-18}	<i>CH NH</i> rocking	1340 ^e , 1337 ^f
	1441.96	1.44×10^{-17}	<i>NH</i> rocking	1423 ^e , 1423 ^f
	1498.97	2.56×10^{-17}	<i>NC</i> stretching	1475 ^e , 1475 ^f
	1564.29	2.79×10^{-17}	<i>CC</i> stretching	1540 ^e , 1539 ^f
	1632.35	2.27×10^{-17}	<i>NH₂</i> scissoring	1602 ^e , 1598 ^f
	1683.00	8.38×10^{-17}	C=C stretching	1659 ^e , 1656 ^f
	1768.89	1.29×10^{-16}	C=O stretching	1730 ^e , 1733 ^f
	3192.84	4.31×10^{-19}	CH stretching	
	3218.01	3.65×10^{-19}	CH stretching	
	3599.58	1.49×10^{-17}	<i>NH₂</i> symmetric stretching	3457 ^e , 3441 ^f
	3617.97	1.17×10^{-17}	NH stretching	3474 ^e , 3472 ^f
	3731.43	8.41×10^{-19}	<i>NH₂</i> antisym. stretching	3575 ^e , 3564 ^f
	142.68	1.45×10^{-19}	CN bending out of plane	
	162.29	4.80×10^{-20}	CNC bending out of plane	
	388.06	3.42×10^{-18}	C=O bending	374 ^a , 391 ^b
	390.53	4.54×10^{-18}	CCN bending	395 ^a , 393 ^b
	521.16	3.42×10^{-18}	skeletal deformation	512 ^a , 516 ^b , 516.5 ^c
	542.13	1.37×10^{-18}	skeletal deformation	536.4 ^b , 536 ^c
	551.96	6.92×10^{-18}	NH bending	545 ^a , 551.2 ^b , 550 ^c
	559.47	6.91×10^{-19}	skeletal deformation	559 ^b , 559 ^c
	670.10	1.42×10^{-17}	NH bending	660 ^a , 662.2 ^b , 662 ^c
	724.44	1.61×10^{-18}	CH bending	717 ^a , 717.4 ^b , 717 ^c
	755.15	8.00×10^{-18}	C=O bending out of plane	757 ^a , 756.5 ^b , 757 ^c
	767.54	5.81×10^{-19}	ring deformation	

Uracil	811.05	9.97×10^{-18}	CH bending	802 ^a , 804 ^b , 804 ^c
	963.84	1.857×10^{-18}	ring stretching	952 ^a , 958.3 ^b , 958 ^c
	965.78	1.19×10^{-19}	CH bending	972 ^a , 981.5 ^b , 982 ^c
	989.54	1.17×10^{-18}	ring deformation	990 ^a , 987.5 ^b , 987 ^c
	1084.64	8.55×10^{-19}	NH, CH bending	1082 ^a , 1075.5 ^b , 1076 ^c
	1188.31	1.76×10^{-17}	NC stretching	1185 ^a , 1192 ^b , 1176 ^c
	1226.63	2.68×10^{-18}	CH bending	1356 ^a , 1217.4 ^b , 1217 ^c
	1381.18	1.40×10^{-17}	CH bending	1387 ^a , 1388.7 ^b , 1389 ^c
	1404.87	1.31×10^{-17}	NH bending	1400 ^a , 1399.6 ^b , 1399 ^c
	1419.96	8.85×10^{-19}	CH bending	
	1498.28	1.38×10^{-17}	NC stretching	1515 ^a , 1517 ^b , 1472 ^c
	1671.13	1.16×10^{-17}	C=C stretching	1641 ^a , 1644 ^b , 1644 ^c
	1767.68	1.16×10^{-16}	C=O stretching	1756 ^a , 1757.5 ^b , 1758 ^c
	1861.92	1.09×10^{-16}	C=O stretching	
	3203.31	4.44×10^{-19}	CH stretching	
	3243.52	1.86×10^{-19}	CH stretching	3124 ^a
3596.94	1.11×10^{-17}	NH stretching	3436 ^a	
3638.27	1.77×10^{-17}	NH stretching	3484 ^a	
	107.53	9.79×10^{-22}	<i>CH</i> ₃ bending	
	141.81	1.12×10^{-19}	<i>CH</i> ₃ torsion	
	145.54	6.63×10^{-20}	<i>CNC</i> bending	
	276.56	4.40×10^{-19}	<i>CH</i> ₃ bending	
	290.10	2.83×10^{-20}	C-C=C bending	
	389.43	3.25×10^{-18}	O=C bending	
	391.08	3.55×10^{-18}	CCN bending	391 ^c
	460.72	3.17×10^{-18}	skeletal deformation	462 ^a , 455 ^c

Thymine	545.85	1.27×10^{-18}	skeletal deformation	541 ^a , 545 ^d , 540 ^c
	549.47	9.42×10^{-18}	NH bending	541 ^a , 541 ^d , 545 ^c
	606.37	2.17×10^{-19}	skeletal deformation	
	668.18	1.42×10^{-17}	NHbending	689 ^a , 662 ^d , 662 ^c
	732.66	8.90×10^{-19}	CC stretching	
	753.41	7.54×10^{-18}	N-C=N bending out of plane	755 ^a , 754 ^d , 754 ^c
	764.83	1.84×10^{-18}	C=O bending	767 ^a , 764 ^d , 764 ^c
	803.19	8.15×10^{-19}	skeletal deformation	804 ^a , 800 ^c
	906.85	3.09×10^{-18}	CH bending	
	963.85	2.26×10^{-18}	NC stretching	963 ^a , 959 ^d , 959 ^c
	1022.22	3.59×10^{-19}	CH ₃ bending	1031 ^a , 1005 ^d , 1002 ^c
	1066.76	1.78×10^{-19}	CH – 3 bending	1078 ^a , 1087 ^d , 1046 ^c
	1148.81	1.23×10^{-18}	NC stretching	
	1196.20	2.34×10^{-17}	NC stretching	
	1222.69	3.96×10^{-18}	CC stretching	1178 ^a , 1183 ^d , 1184 ^c
	1369.69	1.88×10^{-18}	CH bending	1393 ^a , 1388 ^d , 1389 ^c
	1409.17	3.32×10^{-18}	NH bending	1409 ^a , 1405 ^d , 1406 ^c
	1417.06	1.67×10^{-17}	skeletal deformation	
	1422.89	7.68×10^{-19}	CH ₃ bending	1463 ^a , 1433 ^d , 1433 ^c
	1469.28	1.33×10^{-18}	CH ₃ torsion	1463 ^a , 1455 ^d , 1467 ^c
	1490.98	3.26×10^{-18}	CH ₂ scissoring	
	1499.39	9.93×10^{-18}	CH ₂ , CH ₃ bending	1518 ^a , 1472 ^d , 1472 ^c
	1695.39	8.12×10^{-18}	C=C stretching	1668 ^a , 1684 ^d
	1752.45	1.08×10^{-16}	C=O stretching	1725 ^a , 1712 ^d , 1725 ^c
	1798.79	1.34×10^{-16}	C=O stretching	1772 ^a , 1768 ^d , 1769 ^c
	3033.28	3.64×10^{-18}	CH ₃ symmetric stretching	2984 ^a , 2971 ^d

	3085.94	1.66×10^{-18}	CH_2 symmetric stretching	
	3108.20	2.39×10^{-18}	CH_3 antisym. stretching	
	3192.61	8.40×10^{-19}	CH stretching	3076 ^a , 2992 ^d
	3596.29	1.10×10^{-17}	NH stretching	3437 ^a , 3434 ^d , 3434 ^c
	3639.61	1.72×10^{-17}	NH stretching	3484 ^a , 3480 ^d , 3480 ^c
$C_4N_3OH_5$	127.65	7.98×10^{-20}	CNC bending	
	150.03	3.36×10^{-21}	CNC bending	
	376.36	5.18×10^{-18}	NH bending	
	385.65	7.42×10^{-18}	NCC bending	
	511.79	4.37×10^{-18}	NH bending	
	518.60	1.32×10^{-18}	Ring deformation	
	537.81	4.50×10^{-19}	Skeletal deformation	
	560.50	1.70×10^{-18}	Ring deformation	
	585.53	9.75×10^{-18}	NH bending	
	690.21	5.27×10^{-18}	CCC bending	
	749.65	1.19×10^{-17}	C=O bending	
	771.93	6.98×10^{-19}	ring deformation	
	785.09	1.12×10^{-17}	CH bending	
	824.37	4.38×10^{-18}	NH torsion	
	961.25	8.90×10^{-20}	CH bending	
	968.66	3.36×10^{-18}	C-C stretching	
	988.55	4.87×10^{-19}	Ring deformation	
	1072.57	6.62×10^{-18}	NC stretching	
	1144.44	4.16×10^{-18}	NH bending	
	1206.67	2.36×10^{-17}	CH, NH bending	
1270.31	1.47×10^{-17}	NC stretching		

1398.63	4.87×10^{-18}	CH NH torsion
1420.61	4.56×10^{-18}	NH bending
1427.43	1.01×10^{-17}	C-C stretching
1491.01	1.49×10^{-17}	N-C stretching
1665.11	1.57×10^{-18}	C=c stretching
1714.15	8.02×10^{-17}	N=C stretching
1794.22	1.33×10^{-16}	C=O stretching
3208.87	5.19×10^{-19}	CH stretching
3243.95	2.60×10^{-19}	CH stretching
3473.69	1.50×10^{-18}	NH stretching
3604.26	6.64×10^{-18}	NH stretching
3646.48	1.81×10^{-17}	NH stretching

^a Gas phase experiment (Colarusso et al. 1997)

^b Data recorded in neon matrixes (Yu et al. 1995)

^c Data recorded in argon matrixes (Lés et al. 1992)

^d Data recorded in neon matrixes (Graindourze et al. 1990)

^e Data recorded in neon matrixes (Kwiatkowski et al. 1996)

^f Data recorded in argon matrixes (Kwiatkowski et al. 1996)